Numerical Study of a Hybrid Optical DMT/DFT-S QAM Modulation

Amin Yekani and Leslie A. Rusch

IEEE/OSA Journal of Lightwave Technology, (accepted October 2018)

Doi: 10.1109/JLT.2018.2881380

https://ieeexplore.ieee.org/abstract/document/8534352

Numerical Study of a Hybrid Optical DMT/DFT-S QAM Modulation

Amin Yekani, *Member, IEEE,* and Leslie A. Rusch, *Fellow, OSA*, *Fellow, IEEE*

***Abstract*—A hybrid modulation offers the peak-to-average power ratio (PAPR) robustness of discrete Fourier transform spread (DFT-S) QAM (quadrature amplitude modulation) with the bit rate optimization of discrete multi-tone (DMT) modulation. We examine via simulation under what circumstances this hybrid can increase achievable bit rate. Hybrid PAPR reduction allows us to increase the peak-to-peak voltage at the modulator electrical input to increase the signal mean power at the modulator output. We propose a methodology to identify the optimal driving strategy. We optimize the bit rate for the available spectrum, i.e., the spectral efficiency, taking into account the bandwidth limited nature of the transmitter.**

The final optimization we propose is the partition of the available spectrum into a lower frequency band for DFT-S QAM and a higher frequency band for DMT. The modulation level of the DFT-S QAM is also optimized. We compare the optimal hybrid performance versus DMT performance for a range of bit rates for a given modulation bandwidth. Improved performance comes at the cost of greater DSP complexity for the hybrid solution. We compare the number of complex multipliers required to implement hybrid versus DMT for both dispersive and non-dispersive systems.

***Index Terms*—DMT, QAM, DFT-spread, hybrid, simulation, frequency optimization, complexity comparison.**

I. Introduction

EVER growing demand for network capacity requires increased link speed. This requirement attracts research groups to enhance digital signal processing techniques by designing new modulation formats to increase spectral efficiency, equalize non-flat frequency response, and so on. Discrete multi-tone (DMT) and discrete Fourier transform spread (DFT-S) QAM (quadrature amplitude modulation) are two contrasting approaches to this challenge.

DMT divides available spectrum into narrowband subchannels, and uses waterfilling techniques to optimally allocate modulation order and power across these subchannels. With knowledge of the signal-to-noise ratio (SNR) per subchannel, we can maximize channel capacity. DMT suffers from high peak to average power ratio (PAPR), leading to higher levels of quantization noise [1] and amplifier-induced nonlinearities, as compared to other modulations [2]. The most common method to reduce PAPR is clipping, this distortion being milder than that induced by high PAPR [3].

DFT-S modulation allows frequency domain precompensation, a kind of power allocation not unlike DMT. The PAPR of DFT-S modulation is much lower than that of DMT. This method recently achieved 560 Gbit/s with intensity modulation and direct detection (IM/DD), where four wavelength channels used DFT-S 128QAM for a 2 km transmission [4].

Unlike DMT modulation, DFT-S cannot assign a non-uniform number of bits per frequency subdivision, as modulation occurs in the time domain before the fast Fourier transform (FFT). This precludes DFT-S from maximizing capacity. Combining DFT-S with DMT in a hybrid modulation we can seek PAPR reduction (as compared to DMT alone), while enhancing spectral efficiency (as compared to DFT-S alone). This approach was used with IM/DD when combining PAM and DMT [5], and combining OFDM with PAM in a hybrid fiber-visible laser light system [6].

Despite these IM/DD demonstrations, the increase in complexity of hybrid modulation can be difficult to justify in cost-sensitive short haul applications. Coherent detection systems over metro or long haul are more suitable for hybrid DMT/DFT-S modulation. Hybrid modulation experiments were recently reported with 25 Gb/s vertical cavity surface emitting laser technology in [7] using direct detection, and in our work with a silicon photonics Mach Zehnder IQ modulator [8] with coherent detection. No systematic evaluation of the advantages of the hybrid in coherent detection has yet appeared for these systems.

In this paper we study the optimization of joint DMT and DFT-S QAM modulation to increase bit rate, and/or spectral efficiency in coherent detection systems. We provide a technique to find optimal hybrid modulation parameters. We study the trade-off between modulator nonlinearity (induced by high PAPR) and AWGN noise in terms of modulator optical output power or electrical input peak-to-peak voltage (V_{pp}). From this study we derive a driving strategy that minimizes BER for a hybrid modulation, while taking into account the bandwidth limited nature of the transmitter. We propose a partition of the available spectrum into a higher frequency band for DMT and a lower frequency band for DFT-S (at optimized QAM modulation level). We compare the performance of optimal hybrid to that of simple DMT for a range of bit rates for a given modulation bandwidth.

Section II starts with the principals of the hybrid approach. We describe the simulation model and transmitter and receiver side DSP. In section III, we study the hybrid of uniform DMT and DFT-S QAM to find V_{pp} yielding minimum BER. In section IV we optimize the modulation order for QAM, as well as the frequency band partition between DFT-S QAM and DMT. In the end of section IV we compare the optimized hybrid with standard DMT. Section V is dedicated to a complexity comparison of hybrid modulation and standard DMT. Section VI offers some concluding remarks.

II. Principles of Hybrid Modulation and Required DSP

Unlike DMT, PAPR for single carrier modulation can be very low. PAPR varies with pulse shaping; for raised cosine

pulse shaping, PAPR is lowest for rectangular pulses and largest for sinc pulses (also known as Nyquist pulses). While Nyquist pulses have the highest PAPR, they have the best spectral efficiency, equal to that of DMT.

DFT-S is a frequency domain implementation of the Nyquist single carrier approach - an alternative to raised cosine approximations to the sinc pulse. With DFT-S, QAM data is generated in the time domain and moved to the frequency domain using a fast Fourier transform (FFT). In the frequency domain we sculpt frequency occupancy, also constraining it to a limited bandwidth. An inverse fast Fourier transform (IFFT) moves data back to the time domain. Sculpting the signal in the frequency domain helps us to adapt the waveform to channel characteristics.

As explained in the introduction, we create a hybrid modulation by combining DFT-S QAM signal in lower frequencies (where the frequency response is almost flat and the lack of bit allocation is less critical) and DMT in higher frequencies. The single carrier DFT-S QAM part of the combination lowers PAPR (compared to DMT), and the DMT part of helps us maximize throughput (compared to DFT-S QAM) using proper bit allocation and power allocation. Details of this combination is explained in this section. We present our simulation model and our estimation of SNR (per subchannel in the case of the DMT part). We describe transmitter side DSP for signal sculpting, as well as receiver side DSP. The description covers hybrid modulation; when the DFT-S part is set to zero, it covers standard DMT as well.

A. Simulation Model

Figure 1 shows the the simulation model, transmitter side DSP, and receiver side DSP for the hybrid modulation format. The simulator introduces nonlinear behavior in the digital to analog conversion and the sinusoidal transfer function of the modulator. The only noise sources are additive white Gaussian noise (AWGN).

The first block in our simulation model is a digital to a converter (DAC) with high resolution (8-bit) and a 64 GSample/s sampling rate. The bandwidth limitations of the DAC and modulator are simulated with a single low pass Gaussian filter. The modulator is biased at the null point and has the typical sinusoidal transfer function, normalized so that the maximum amplitude input voltage of $V_\pi/2$ generates an output signal equal to one. The mismatch between the local oscillator and the transmit laser is modeled with a random frequency offset, uniformly distributed between 0 and 500 MHz. The laser is modeled as having phase noise described by a Wiener process and parameterized by a 100 kHz linewidth. Finally, AWGN is added to reflect the noise level being examined. The key simulation parameters are summarized in Table I.

TABLE I
KEY SIMULATION PARAMETERS

Parameter	Value
DAC	28-bit + 64 GSample/s
Laser	Phase noise with Wiener process (LW = 100 kHz)
Modulator	LPF + Transfer function nonlinearity
Frequency offset	Random number between 0-500 MHz

B. Transmitter DSP

Before starting transmitter-side DSP, we estimate the SNR that will be used for waterfilling and for power allocation between the DMT and the DFT-S QAM portions of the spectrum. In this block, we fix the percentage of available spectrum allocated to DFT-S QAM, illustrated as a block of N_{QAM} subchannels at baseband, and N_{DMT} subchannels at higher frequency. We then run a simulation transmitting QPSK signals with uniform power allocations for DFT-S QAM and DMT. DMT subchannels with the same power level and modulation (QPSK), i.e., uniform DMT is also known as orthogonal frequency division multiplexing (OFDM). At the receiver we estimate the SNR per subchannel for the DMT spectra, and overall SNR for the DFT-S QAM spectrum using techniques described in [9]. This is repeated for each partitioning of the spectrum that we examine.

The total FFT size is $N_{FFT} = N_{DMT} + N_{QAM}$, as illustrated in Fig. 1. The ratio N_{FFT}/N_{QAM} gives the percentage of spectrum allocated to DFT-S QAM. The transmitter side DSP starts with generating a pseudo-random bit sequence (PRBS) of order 22. For a fixed hybrid (DFT-S QAM modulation level and percentage of spectrum), we divide the bit sequence appropriately between the two branches in the TX DSP section of Fig. 1.

For a fixed hybrid (modulation order for DFT-S and N_{QAM}), we calculate the power allocation for the DFT-S partition as the amount of power needed to achieve a target BER of 10^{-3} based on overall QAM SNR. For the DMT portion, we use Chow's waterfilling algorithm [10], to allocate power again with target BER of 10^{-3}. The bit allocation step of waterfilling [10] spreads the DMT bits among subchannels (N_{DMT} in Fig. 1) to achieve the target bit rate. Target bit rate is adjusted to find the highest bit rate achievable.

Modulated QAM symbols for the DFT-S spectrum are moved to the frequency domain with a fast Fourier transform (FFT) block. In the frequency domain the DFT-S data is concatenated with DMT data to fill the entire available spectrum as illustrated in cartoons in Fig. 1. Finally, a preamble is added for frequency offset estimation. The frequency domain signal is moved to the time domain using an inverse fast Fourier transform (IFFT) block. The last stage is parallel to serial conversion.

C. Receiver DSP

The receiver side DSP starts with an FFT block to move the time domain signal into the frequency domain. We then apply frequency offset compensation (FOC) using the Schmidel-Cox algorithm [11]. After FOC, we separate QAM data from DMT. In the DMT side we apply carrier phase recovery (CPR), then one tap equalization and finally we estimate BER.

For the QAM data, we first pass through a parallel to serial block. We then apply blind channel equalization using an N_1 tap multi-modulus algorithm (MMA) at two samples per symbol [12]. We next down sample the data to one sample

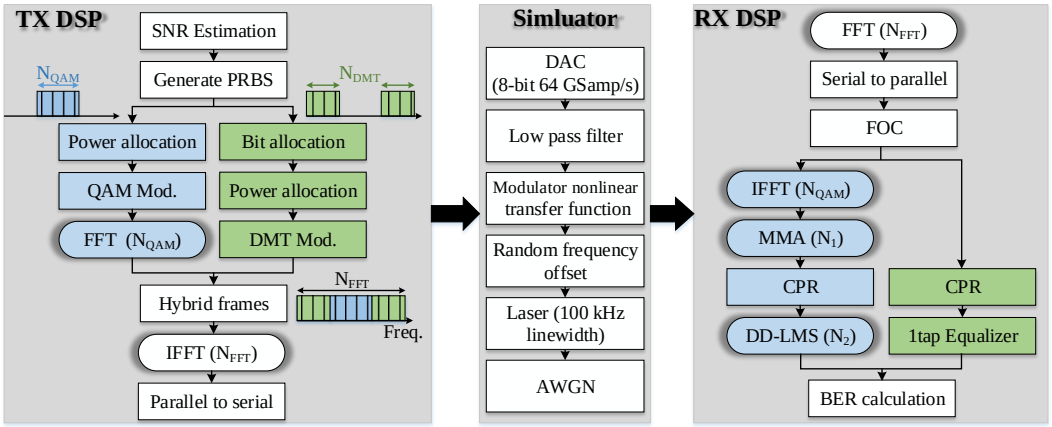

Fig. 1. Monte Carlo simulation block diagram (center panel) and flowcharts for hybrid modulation for transmitter-side (left panel) and receiver-side (right panel) DSP.

per symbol and go into the CPR block. After CPR we apply a N_2 tap decision-directed least mean square error (DD-LMS) equalizer and finally we calculate BER.

We used the same CPR technique for both QAM and DMT. We use a small portion of the data in each frame (1/30) to estimate phase rotation for that frame. This estimated phase is applied to all samples of the frame. This method has lower complexity than blind search [13] or other CPR methods. Bit error rate was estimated via Monte Carlo methods, testing 2×10^7 bits and counting a minimum of 20 errors.

III. Driving Strategy for Hybrid Modulation

In this section, we show that increasing the DFT-S portion of the hybrid decreases the PAPR for the hybrid modulation. Then we study the trade-off between AWGN noise and the modulator nonlinear transfer function. From this trade-off we derive a driving strategy for the modulator to minimize BER for a specific hybrid spectral partition, OSNR value, and modulator bandwidth. Following that we optimize modulation order and frequency occupation for DFT-S portion for a fixed bit rate. Finally we find the maximum bit rate under the forward error correction (FEC) threshold for optimized hybrid modulation and compare it to standard DMT.

A. Impact of hybrid spectral partition on PAPR

As explained in the introduction, the main reason to combine DFT-S QAM and DMT is to reduce PAPR. Quantization noise is negligible when using a high resolution (8-bit) DAC, but transfer function nonlinearity can be severe in the presence of high PAPR. The nonlinear distortion is most severe for large excursions from the mean value. The higher the PAPR, The greater the probability of such excursion occurring. The probability of the excursion above the mean is a good predictor of PAPR impact. Typically, excursions of 9.5 dB above the mean value are considered to generate excessive nonlinear distortion.

In Fig. 2 we plot the probability of exceeding the mean by a certain excursion level in dB for three hybrid spectral partitions. In the first case we generate uniform DMT, second one is a combination of 50% DMT and 50% DFT-S QAM, and the last one is all DFT-S QAM.

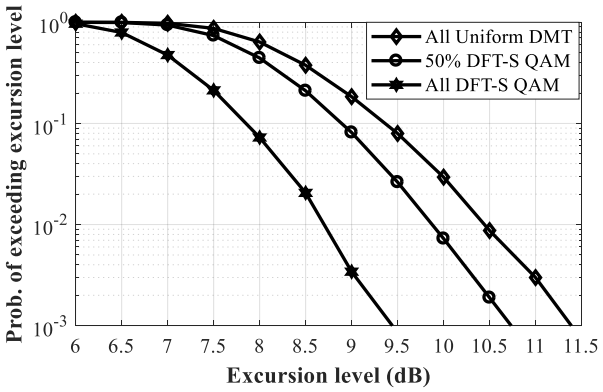

Fig. 2. Probability of exceeding at any instance a certain level of excursion from the signal mean value for: strictly uniform 64QAM DMT, strictly DFT-S 64 QAM, and a hybrid of half spectrum uniform 64QAM DMT and half spectrum DFT-S 64QAM.

Consider the excursion level of 9.5 dB, where nonlinear distortion limits performance. At this level, uniform DMT has 10% of samples distorted. By using a 50-50 hybrid this probability is decreased to 2%. For the case of all DFT-S QAM modulation, only 0.1% of samples are distorted, which is negligible. Clearly DFT-S QAM has lower PAPR, as expected and by adjusting the mix of DMT and DFT-S we can tune the level of PAPR. That is, varying the percentage of DFT-S QAM can shift the plot in Fig. 2 any where between the two extremes of all uniform DMT and all DFT-S QAM.

B. Driving strategy minimizing BER

Nonlinearity induced by the modulator sinusoidal transfer function can be reduced by lowering mean power, i.e., operating at lower V_{pp}. While low V_{pp} reduces nonlinearity, it decreases OSNR as well. Proper choice of V_{pp} balances these two effects to minimize BER. We examine the trade-off to find the optimal driving strategy for two cases: for modulator bandwidth much greater than required for the transmission

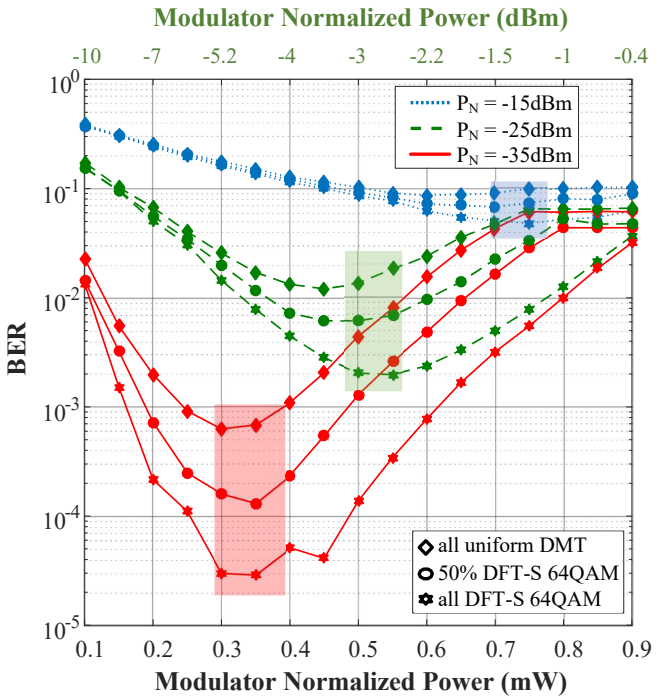

Fig. 3. BER versus normalized modulator output power at three noise levels for: strictly uniform 64QAM DMT, strictly DFT-S 64 QAM, and a hybrid of half spectrum uniform 64QAM DMT and half spectrum DFT-S 64QAM.

rate (infinite bandwidth) and for bandwidth limited operation, i.e., high bit rates. We used Monte Carlo techniques in the simulator shown in Fig. 1 to calculate the BER for each case in this section.

1) Influence of noise level for infinite bandwidth: In this subsection we continue to use uniform DMT, leaving power and bit allocations for following sections. The low pass filter in Fig. 1 is not present for simulations of this infinite bandwidth case. The noise levels are fixed for the simulation. In this way we can set the noise level independently of the bandwidth assumption.

Figure 3 shows the BER versus normalized modulator output power for three values of noise power (P_N): -35 dBm, -25 dBm, and -15 dBm. We swept normalized modulator output power by changing the peak-to-peak voltage, while we fixed the bias at the null point. For each value of P_N we consider the three modulations for which we found the PAPR cumulative distribution function in Fig. 2.

Lowering PAPR with a fixed OSNR reduces the effect of modulator transfer function nonlinearity, decreasing the BER. This effect can be seen no matter the level of P_N. This is also true when sweeping the x-axis. The BER performance is best for full DFT-S QAM, followed by the 50% hybrid, and uniform DMT has the worst performance. The BER trend follows the PAPR cumulative distribution function.

Consider the optimum values for modulator output power for all nine cases shown in Fig. 3. The optimum value changes significantly with the noise level. For a fixed noise level, however, the minimum BER occurs at roughly the same normalized modulator power no matter the PAPR level, i.e, no matter the hybrid partition. The optimum region of normalized modulator power is shaded for each noise power case, e.g., the red region (around 0.35 mW) covers the case of $P_N = -35$ dBm. If we increase noise level by 10 dB the optimum value increases to around 0.55 mW. Greater modulator output power is required as we are AWGN noise limited rather than PAPR limited. Further increase in noise power up to -15 dBm increases the optimum value of modulator output power to around 0.75 mW.

Limiting the bandwidth of the system could reduce PAPR of the signal by attenuating higher frequencies and avoiding sudden changes in the amplitude of the signal. For different values of modulator bandwidth the value of OSNR will be the same if we keep modulator output power unchanged. Therefore we expect changing system bandwidth should have negligible effect on the optimum value of modulator output power, for the same reasons this was the case when changing the hybrid spectral partition between DFT-S and DMT. We examine this hypothesis in the following.

2) Influence of noise level for finite bandwidth: For the rest of the paper our simulator includes a low pass Gaussian filter with a 3 dB bandwidth of 25 GHz. When the system bandwidth is limited, optimized DMT uses waterfilling to adapt the signal to the channel frequency response, thus outperforming uniform DMT. For the balance of the paper, we maximize capacity by allocating the appropriate power and number of bits per symbol at each subchannel.

The AWGN noise power is set to -33 dBm, a reasonable value for a 25 GHz receiver. From Fig. 3, at this noise level the modulator normalized power should be around 0.4 mW to minimize BER, regardless of hybrid split or the system bandwidth. This modulator output power corresponds to 29 dB OSNR, which is a reasonable value for a back-to-back experiment.

Figure 4 shows the BER versus modulator output power for four different hybrid combinations, all of which achieve a bit rate of 260 Gb/s. The DFT-S 64QAM portion of the four hybrid modulations examined has bit rate varying from 100 Gb/s to 240 Gb/s; the balance of the 260 Gb/s is covered by the waterfilled DMT. The percentage noted beside the curve gives the DFT-S QAM bandwidth as a percentage of the total bandwidth covered by the FFT (64 GHz in our simulations). Figure 4 confirms that the optimal modulator output power is around 0.42 mW, which is in less than 0.1 mW range from what we predicted for infinite bandwidth in Fig. 3. While not reported here, we confirmed the same behavior for a variety of system bit rates and bandwidths. In all cases, the optimum modulator output power is not affected by the hybrid spectral allocation, nor by the system 3 dB bandwidth.

IV. Optimizing Bit Rate

By changing the hybrid spectral allocation to place the split between DMT and DFT-S QAM at higher frequencies, we increase the DFT-S portion and decrease the PAPR of the overall signal. Lower PAPR means lower nonlinear distortion and better performance. Placing the split point too high leads to limited bandwidth to meet DMT bit rate targets. This will force the waterfilling to go to advanced QAM orders that

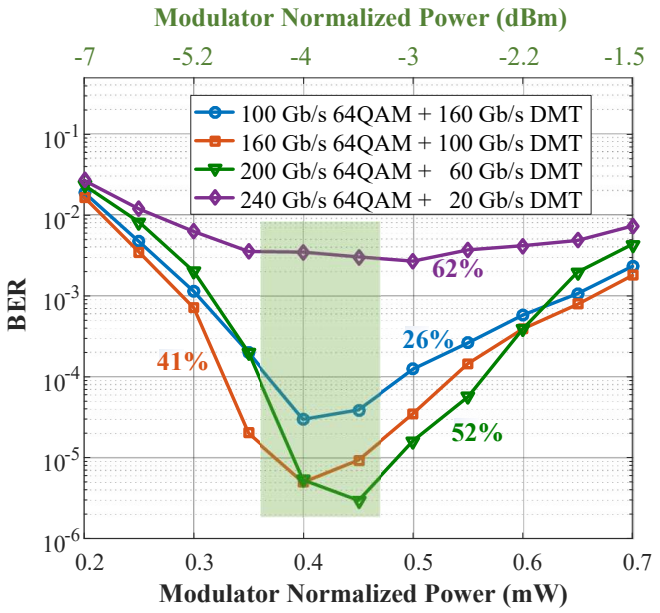

Fig. 4. For overall bit rate of 206 Gb/s, noise power of -33 dBm, and 25 GHz system bandwidth: BER versus normalized modulator output power for four different hybrid spectral allocations.

require strong SNR. At these high frequencies, however, the SNR will be limited as the channel rolls off. This is reflected in Fig. 4 where we see BER improvement until 52%, and a rapid deterioration at 62%.

In the first subsection, we find the optimal split point assuming a fixed QAM level for the DFT-S QAM section. This optimization is done for each candidate QAM level. For a given overall bit rate, we identify the best split point and QAM order to minimize BER. We compared the optimized hybrid with DMT for different bit rates in the second subsection. As previously, the OSNR is 29 dB, modulator output power is 0.4 mW, and system 3 dB bandwidth is 25 GHz.

A. *Fixed QAM level for DFT-S*

We fix the overall bit rate to 320 Gb/s and examine three candidate levels for the DFT-S QAM partition: 32QAM, 64QAM, and 128QAM. We next sweep the hybrid spectral partition and find the BER for that hybrid modulation. Figure 5 plots, a) BER and b) QAM power portion vs. the hybrid partition. The lower x-axis is keyed to the bandwidth allocated to DFT-S QAM, while the upper x-axis gives this frequency as a percentage of the total bandwidth covered by the FFT (again, 64 GHz). For example, for DFT-S 64QAM with 20 GHz bandwidth, the bit rate for DFT-S 64QAM is $20 \times 6 = 120$ Gbit/s and the DMT bit rate is $320 - 120 = 200$ Gbit/s. The three curves in Fig. 5 are for 32QAM, 64QAM, and 128QAM, shown by red (circle marker), green (triangle marker), and blue (square marker) lines, respectively.

The dashed horizontal line in Fig. 5a is a reference point for the BER when using strictly DMT with waterfilling and no DFT-S QAM. We observe that for higher QAM modulations (64 and 128), there is a clear optimum hybrid spectral allocation minimizing BER. At 32QAM, the BER curve is

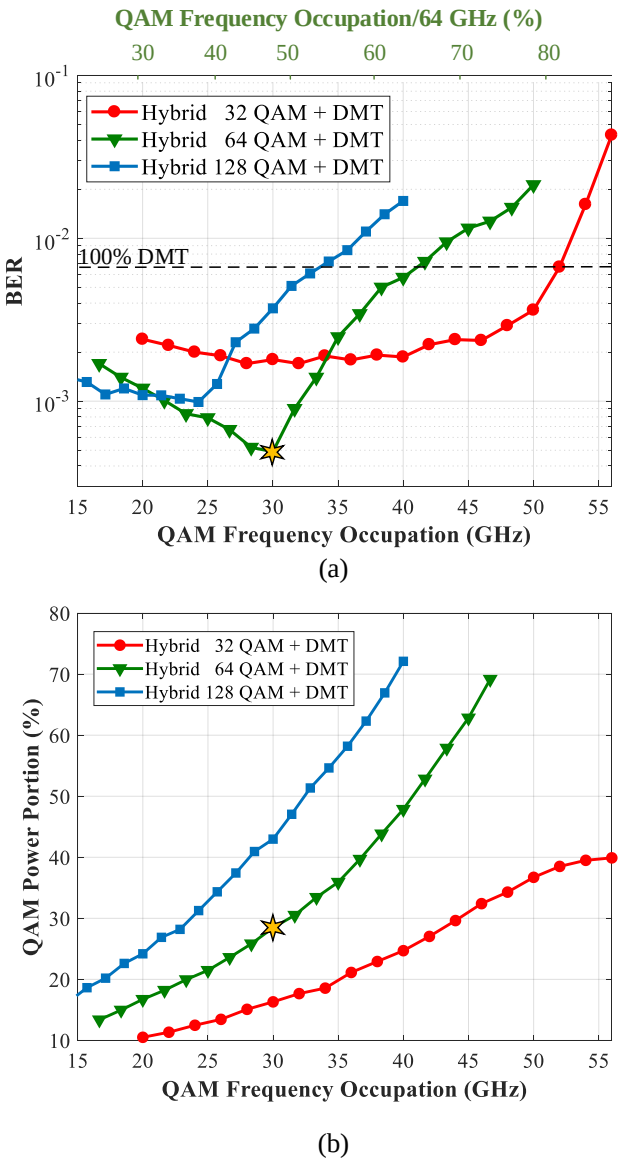

Fig. 5. a) BER and b) QAM power portion, each versus DFT-S QAM frequency occupation for three different choices of QAM order; 320 Gb/s overall bit rate, -33 dBm noise power, 25 GHz system bandwidth, and 0.42 mW modulator output power.

very shallow, with a range of QAM frequency occupation achieving best BER. In Fig. 5b we plot the percentage of power allocated to QAM as a function of QAM frequency occupation. The percentage grows monotonically, as a greater portion of spectrum requires more power. As higher order DFT-S QAM has greater sensitivity to AWGN, the curve is highest for 128QAM, lowest for 32QAM. We see in Fig. 5b that for 32QAM the power allocation to QAM saturates at 40%; in this region DMT can exploit its flexibility to go to higher order modulations. For 32QAM, the hybrid performs better than 100% DMT, but does not achieve the gains when QAM is permitted to go to higher orders (64 and 128).

Higher order DFT-S QAM at a given frequency occupation means higher bit rate in the DFT-S QAM part; we have higher spectral efficiency, but more sensitivity to the AWGN. At high

frequency occupation (35% and higher), we see in Fig. 5a the typical relative performance: lowest BER for 32QAM and highest BER for 128QAM. At lower occupation (33% and below), we see the trade-off in the hybrid modulation: lower BER by balancing the PAPR (nonlinear) and AWGN (linear) impairments.

More power devoted to QAM means more PAPR reduction; at the same time, it reduces the DMT power allocation making it harder to achieve the DMT BER target. This trade-off is visible in the intersecting curves and clear minima (64QAM and 128QAM cases) in Fig. 5a BER curves. For instance, at 22 GHz the curves for 64QAM and 128QAM BER intersect. Above 22 GHz DFT-S 64QAM is a better choice, as DMT does not have enough resources (power and spectrum) to overcome the restrictions imposed by noise sensitivity in DFT-S 128QAM. The minima occur when the two DMT effects (PAPR advantage, power allocation disadvantage) balance.

Returning to 32QAM, this is clearly not a good choice for the 320 Gb/s target. The flat p art o f t he c urve s hows there is a balance in reduced PAPR and limited DMT frequency range. For 320 Gb/s, the best choice is 64QAM with 30% QAM frequency occupation, as shown in Fig. 5a and 5a by a gold star. Despite the nonlinear curves in Fig. 5b, the optimal power allocation happens to be about 30% (y-axis) as well.

B. Best hybrid for bit rate

We repeated the optimization procedure described in the last subsection as we swept bit rates. The highest modulation level for a DMT subchannel was 128QAM, hence the modulation levels we examined for DFT-S QAM were sufficient to cover achievable performance. Figure 6 shows a plot of BER for the best choice of hybrid configuration in red (star markers). The maximum bit rate under the FEC threshold of 3.8e-3 (7% overhead hard decision FEC) for DMT alone is 320 Gb/s. This rate increases to 360 Gb/s if we use hybrid modulation. As the bit rate decreases, the performance enhancement of the hybrid decreases. Pushing to these aggressive bit rates in a 64 GHz bandwidth (see spectral efficiency given in upper axis), requires a DMT portion with a high bit allocation. However, including more DMT leads to less the PAPR reduction.

Figure 7 shows the hybrid spectral allocation that yielded the best performance for each bit rate, i.e., the DFT-S frequency occupation for the points in Fig. 4. From 260 to 340 Gb/s, the best constellation for DFT-S QAM is 64QAM. Above 340 Gb/s, it is better to reduce frequency occupation and increase QAM order to send more bits over a smaller frequency range; DMT waterfilling over more frequency bins allows the bit rate to grow.

C. Experimental validation

In [8], we reported an experimental investigation of the hybrid modulation, but without optimization of the driving strategy outlined in section III. In that experiment, we examined only 16QAM for the DFT-S portion, but at three different frequency occupations. The 100% DMT case was also examined. We used a silicon photonic traveling wave

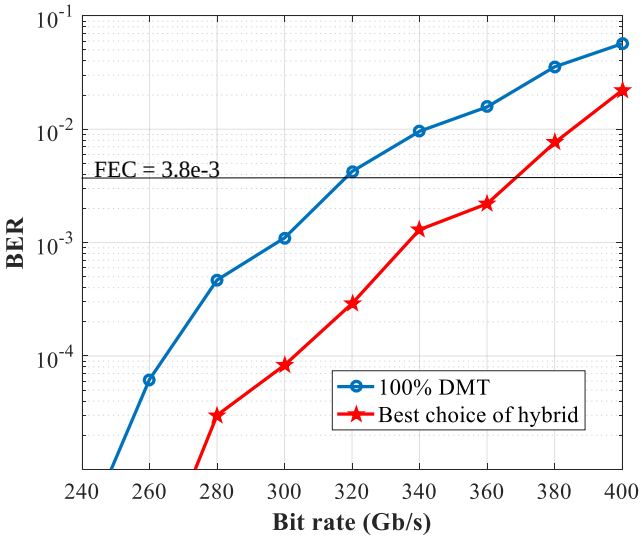

Fig. 6. For noise power of -33 dBm, 25 GHz system bandwidth, and modulator output power of 0.42 mW: BER versus bit rate for 100% DMT (blue circle markers) and best choice of hybrid (red star markers).

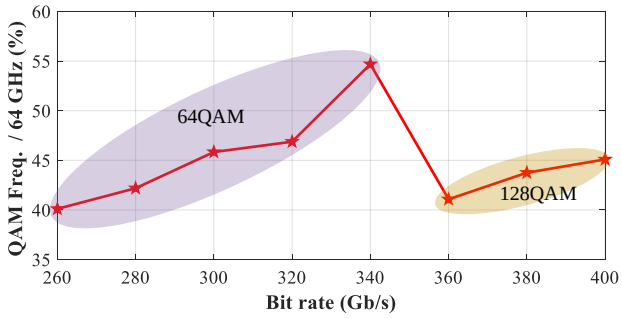

Fig. 7. For noise power of -33 dBm, 25 GHz system bandwidth, and modulator output power of 0.42 mW: Best hybrid spectral allocation for targeted bit rates; best DFT-S QAM modulation was 64QAM for bit rates up to and including 340 Gb/s, 128QAM at 360 Gb/s and higher.

modulator with a 3 dB bandwidth of 20 GHz. Due to coupling losses, the OSNR was limited to 23 dB. The 20 GHz band and was divided into 256 subbands for the hybrid modulation; a total of 120 Gb/s was transmitted.

Details of our experimental setup are provided in section III of [8], while Fig. 8 shows the BER versus bit rate achieved. Pure DMT (blue, circle markers) has higher error rate than all three hybrid modulation scenarios. When sweeping the DFT-S frequency occupancy from 25% to 35% we can see the importance of PAPR mitigation peaking and diminishing. From 25% occupancy (representing 64 Gb/s of the total 120 Gb/s) we increase to 31% (80 Gb/s) to see the best performance. Increasing occupancy beyond this point leads to a small power allocation to DMT that causes a decrease in performance. At 35% occupancy, the hybrid performance is worse than pure DFT-S, *i.e.*, DMT is not helping. This validates our simulation results in Fig. 5a, where we have an optimum QAM frequency occupation.

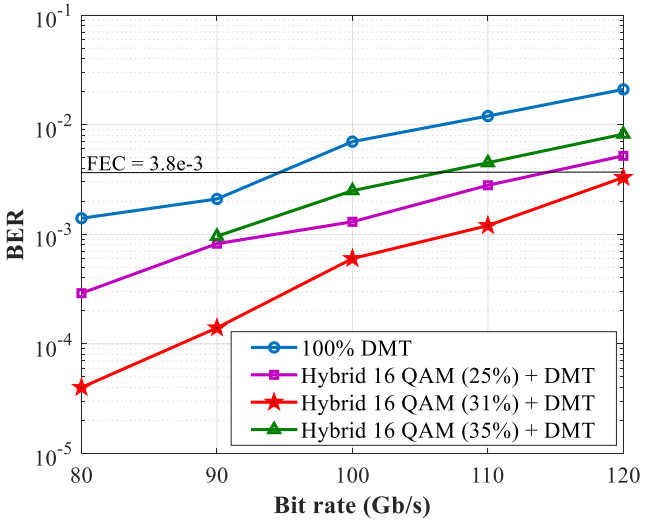

Fig. 8. Experimental comparison [8] at 120 Gb/s between pure DMT and three hybrid modulations with different DFT-S frequency occupations; the driving strategy in section III is not used in experimentation.

V. Complexity Increase with Hybrid

Using a hybrid modulation format enhances system performance, but requires additional DSP blocks for both DMT and QAM subsystems. Such extensive DSP increases the complexity and implementation cost. In this section, we calculate the complexity of hybrid modulation and compare it to DMT. We first identify DSP blocks that represent the largest portion of processing complexity, and then focus on the the complexity for these blocks.

Whether implemented in an application specific integrated circuit (ASIC) or a field programmable gate array (FPGA), the latency of a multiplier is greater than that of an adder. But more importantly, the cost and chip space of a multiplier is much higher than that of an adder. Therefore, we restrict our complexity analysis to the number of multipliers per bit.

In the next subsections we assume zero dispersion, and focus on the complexity of hybrid modulation alone. In the final subsection, we discuss how a dispersion compensation block impacts the overall complexity when using a hybrid.

A. Common and negligible DSP operations

The DSP tasks in Fig. 1 are formatted to identify DSP relevance to our comparison of complexity. All white boxes are DSP needed for both QAM and DMT modulations and are not considered as additional complexity vis-á-vis standard DMT. DSP blocks unique to DFT-S QAMor DMT are shown with blue and green boxes, respectively.

Blocks with high complexity are shown with rounded edges in Fig. 1. On the transmitter side, we have an FFT stage for the DFT-S QAM DSP flow, and an IFFT block for the hybrid signal that contribute significantly to complexity. On the receiver side, system complexity is determined by the FFT stage for hybrid signal, and the IFFT block and MMA and DD-LMS equalizers for the DFT-S QAM DSP flow.

To decrease complexity of implementing hybrid modulation we can share the FOC block. The offset estimation is performed after the initial FFT and before splitting the subchannel data between the two DSP flows. We use two frames as a preamble for frequency offset estimation and compensation. Implementing the FOC in an ASIC is simple and could be neglected compare to the other DSP sections [14].

The carrier phase recovery stage was explained in previous sections. We use a training-symbol-based (data aided) algorithm, with a single phase shift for each frame of data for both DMT and DFT-S QAM. The complexity of this CPR method is much lower than that of the blind equalization blocks (MMA or DD-MLS), and therefore it can be neglected in our complexity comparison.

B. Implementation complexity of main contributors

Next we calculate number of complex multipliers for DSP blocks with high complexity and estimate the overall complexity for hybrid and DMT. Blocks with dominant DSP complexity in this paper can be divided in two categories: FFT/IFFT and equalizers. In the next two subsections we calculate number of complex multipliers per signal symbol (CPS) in FFT/IFFTs and equalizers.

1) FFT + IFFT: The implementation complexity for FFT and IFFT are the same. Each requires $N\log_2(N)/2$ complex multipliers implemented with a radix-2 algorithm, where N is the smallest power of two greater than or equal to the target FFT length. For highest efficiency of hardware resources, we choose a power of two for FFT size. Radix-4 is can be used to implement the FFT and requires only $3N\log(N)/8$ multipliers; however, requiring a power of four limits the options for FFT size even more [15], [16]. We chose the popular radix-2 algorithm for its popularity and greater freedom in choosing FFT length. CPS for a combined FFT and IFFT blocks is

$$CPS_{FFT+IFFT}^{radix-2} = 2 \times \log_2(N)/2 = \log_2(N). \quad (1)$$

2) Equalizer: Any equalizer can be implemented in the time domain (TDE) or the frequency domain (FDE). The computational complexity for FDE is much lower than TDE [17], [18], so we consider only FDE for our comparison.

Consider a frequency domain equalizer with N_{eq} taps and N_{SPS} samples per symbol. To obtain N_{eq}/N_{SPS} output symbols, we need N_{eq} complex multipliers to calculate the equalizer output, and N_{eq} complex multipliers to update equalizer taps. Furthermore, we need to eight length N_{eq} FFTs [15]. The CPS for an equalizer with N_{eq} taps, and N_{SPS} number of samples per symbol using FDE technique is

$$CPS_{EQ}^{FDE} = \left[2N_{eq} + 4N_{eq}\log_2(N_{eq})\right] N_{SPS}/N_{eq} \quad (2)$$

C. Number of multipliers per bit

CPS is a good figure metric for system complexity, but it cannot show the hardware efficiency with bit rate. For such a comparison it is better to calculate the number of required multiplexers per bit (CPB) which is

$$CPB = CPS/(BR/BW), \quad (3)$$

where BR is the overall bit rate of the system, and BW is the overall frequency range covered by DAC (64 GHz in our work). BR/BW shows the number of bits per single symbol that is uploaded to the DAC.

D. Quantifying multiplies/bit

Figure 9 shows the CPB as a function of bit rates for standard DMT (red triangle markers) and our optimized hybrid modulation format (blue triangle markers). We provide a bar chart breakdown of contributions to the CPB for 320 Gb/s. The CPB portions of the DFT-S QAM FFT (transmitter) and IFFT (receiver), the DD-LMS, and the MMA are shown with green, gray, and blue boxes, respectively. In the following we explain details of this complexity calculation and the parameters we chose for different cases.

The overall number of multipliers per bit of the common FFT and IFFT blocks is calculated from (1), and (3). This value is indicated as a red box in the bar chart of Fig.9. We used an FFT size of $N_{FFT} = 1024$ for the common FFT/IFFT blocks. This is the contribution used to trace the DMT complexity curve.

For hybrid modulation, the CPB for all frequency domain equalization and the DFT-S QAM pair of IFFT/FFT is

$$CPB = \frac{6 + 8\log_2(N_1) + 4\log_2(N_2) + \log_2(N_{QAM})}{BR/BW} \quad (4)$$

where N_{QAM} is the smallest power of two greater than or equal to the number of sub-channels dedicated to DFT-S QAM portion. At each bit rate, we used the optimum frequency occupation presented in Fig. 9 to find N_{QAM}. Only two values of N_{QAM} are used: 512 for occupancy below 50%, and 1024 occupancy above 50%.

In our BER simulation reported in previous sections, we assumed a sufficiently large number of taps for equalizers to have the best achievable performance. This led to N_{eq} of 77 for MMA and 43 for DD-LMS. To quantify complexity, we reduced the number of taps until the performance penalty was less than that of a 0.5 dB decrease in SNR. We restricted ourselves to powers of two when finding the reduced number of taps, leading to N_{eq} of 32 for MMA and 16 for DD-LMS. The N_{SPS} for MMA is two and for DD-LMS is one. The bar chart contributions of MMA and DD-LMS reflect these values. Complexity parameters are summarized in table II.

For the swept bit rates, the frequency occupancy of DFT-S QAM only varies from 40 to 55% per Fig. 7. Therefore, the number of multipliers is virtually unchanging across swept bit rates. The CPB (i.e., *per bit*) for the hybrid is decreasing almost linearly with bit rate due to (4) denominator of BR.

TABLE II
PARAMETERS FOR HYBRID MODULATION DSP

Parameter	Value
N_1	32
N_2	16
N_{FFT}	1024
N_{QAM}	512-1024

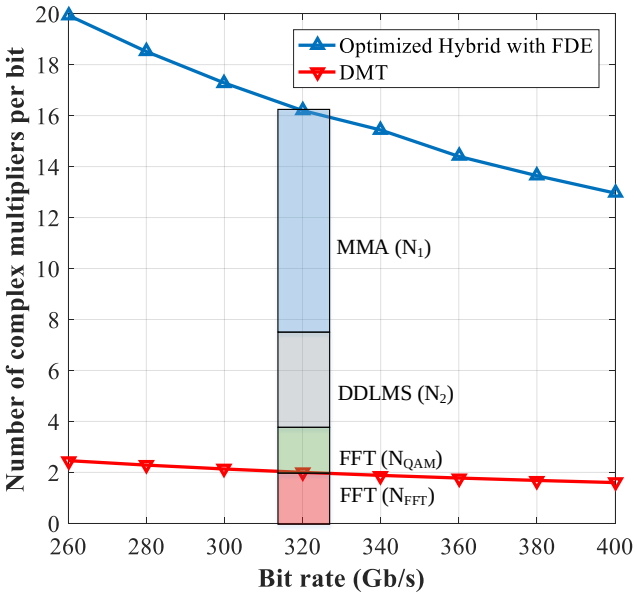

Fig. 9. For system bandwidth of 25 GHz, modulator output power of 0.42 mW and noise power of -33 dBm: Number of complex multipliers per bit of hybrid modulation and DMT modulation versus bit rate.

E. Comparative complexity

The plots in Fig. 9 for different bit rates cover the case of back-to-back communications, i.e., without dispersion compensation complexity included. Comparing the complexity for different blocks at 320 Gb/s bit rate in Fig. 9, the largest portion of the overall multipliers per bit is for the MMA algorithm, in large part this is due to required two samples per symbol. MMA, DD-LMS and DFT-S QAM FFT/IFFT blocks consume 87% of the overall number of complex multiplexers per bit for hybrid modulation. This leads to a large difference between DMT and hybrid complexity for the back-to-back case. The complexity difference becomes smaller as we increase bit rate and use the same hardware to send more bits.

For long haul systems, a chromatic dispersion (CD) compensation block is needed for both hybrid and DMT. This CD bloc has complexity on a par with the rounded blocks in Fig. 1 for longer links. The number of taps for a CD compensation filter from [19] is

$$N_{CD} \approx \frac{LDcRs^2}{4f_c^2}, \quad (5)$$

where L is the fiber length in km, D is the dispersion, f_c is the laser frequency, and R_s is the sampling rate. For $f_c = 193$ THz, $R_s = 64$ Gsamples/s, and $D = 18$ ps/nm·km, we obtain $N_{CD} \approx 0.14L$. For short range, $L < 20$ km, four taps are enough. By increasing fiber length to 285 km we need 40 taps and 10.8 multiplexers per bit at 320 Gb/s to remove CD. In this case, the additional hybrid complexity is only 52% of overall complex multipliers. This percentage becomes smaller with increasing fiber length and makes hybrid a good choice for long haul applications.

VI. Conclusion

We present a numerical study of a hybrid modulation format in which we combine DFT-S QAM for lower frequencies and DMT for higher frequencies. We optimized hybrid modulation for: driving strategy, DFT-S QAM modulation order, and DFT-S QAM frequency spectrum allocation. The performance of the optimized hybrid is compared to that of DMT and we show an improvement with hybrid modulation. The improvement decreases as we increase bit rate in a fixed available bandwidth. The maximum bit rate under hard decision FEC threshold of 3.8e-3 is increased by 40 Gb/s with hybrid modulation instead of DMT. We calculate the number of complex multipliers per bit to compare the complexity between hybrid and 100% DMT. Complexity of hybrid modulation is much higher than DMT for back to back links, but low for links longer than several hundred kilometers.

References

[1] C. R. Berger, Y. Benlachtar, R. I. Killey, and P. A. Milder, "Theoretical and experimental evaluation of clipping and quantization noise for optical OFDM," *Opt. Express*, vol. 19, no. 18, pp. 17 713–17 728, Aug 2011. [Online]. Available: http://www.opticsexpress.org/abstract.cfm?URI=oe-19-18-17713

[2] S. Amiralizadeh, A. T. Nguyen, and L. A. Rusch, "Modeling and compensation of transmitter nonlinearity in coherent optical OFDM," *Opt. Express*, vol. 23, no. 20, pp. 26 192–26 207, Oct 2015. [Online]. Available: http://www.opticsexpress.org/abstract.cfm?URI=oe-23-20-26192

[3] X. Li and L. J. Cimini, "Effects of clipping and filtering on the performance of ofdm," in *1997 IEEE 47th Vehicular Technology Conference. Technology in Motion*, vol. 3, May 1997, pp. 1634–1638 vol.3.

[4] F. Li, J. Yu, Z. Cao, J. Zhang, M. Chen, and X. Li, "Experimental demonstration of four-channel WDM 560 gbit/s 128QAM-DMT using IM/DD for 2-km optical interconnect," *J. Lightwave Technol.*, vol. 35, no. 4, pp. 941–948, Feb 2017. [Online]. Available: http://jlt.osa.org/abstract.cfm?URI=jlt-35-4-941

[5] W. A. Ling, Y. Matsui, H. M. Daghighian, and I. Lyubomirsky, "112 gb/s transmission with a directly-modulated laser using FFT-based synthesis of orthogonal PAM and DMT signals," *Opt. Express*, vol. 23, no. 15, pp. 19 202–19 212, Jul 2015. [Online]. Available: http://www.opticsexpress.org/abstract.cfm?URI=oe-23-15-19202

[6] F. Zhang, J. He, R. Deng, Q. Chen, and L. Chen, "Performance improvement by orthogonal pulse amplitude modulation and discrete multitone modulation signals in hybrid fiber-visible laser light communication system," *Optical Engineering*, vol. 55, pp. 55 – 55 – 5, 2016. [Online]. Available: https://doi.org/10.1117/1.OE.55.10.106106

[7] W. A. Ling, I. Lyubomirsky, R. Rodes, H. M. Daghighian, and C. Kocot, "Single-channel 50g and 100g discrete multitone transmission with 25g VCSEL technology," *J. Lightwave Technol.*, vol. 33, no. 4, pp. 761–767, Feb 2015. [Online]. Available: http://jlt.osa.org/abstract.cfm?URI=jlt-33-4-761

[8] A. Yekani, M. Banawan, and L. A. Rusch, "Flexible modulation and frequency allocations for SNR-limited coherent systems," in *2018 IEEE Canadian Conference on Electrical Computer Engineering (CCECE)*, May 2018, pp. 1–3.

[9] A. Yekani, M. Chagnon, C. S. Park, M. Poulin, D. V. Plant, and L. A. Rusch, "Experimental comparison of pam vs. dmt using an o-band silicon photonic modulator at different propagation distances," in *2015 European Conference on Optical Communication (ECOC)*, Sept 2015, pp. 1–3.

[10] P. S. Chow, J. M. Cioffi, and J. A. C. Bingham, "A practical discrete multitone transceiver loading algorithm for data transmission over spectrally shaped channels," *IEEE Transactions on Communications*, vol. 43, no. 2/3/4, pp. 773–775, Feb 1995.

[11] T. M. Schmidl and D. C. Cox, "Robust frequency and timing synchronization for OFDM," *IEEE Transactions on Communications*, vol. 45, no. 12, pp. 1613–1621, Dec 1997.

[12] I. Fatadin, D. Ives, and S. J. Savory, "Blind equalization and carrier phase recovery in a 16-QAM optical coherent system," *J. Lightwave Technol.*, vol. 27, no. 15, pp. 3042–3049, Aug 2009. [Online]. Available: http://jlt.osa.org/abstract.cfm?URI=jlt-27-15-3042

[13] T. Pfau, S. Hoffmann, and R. Noé, "Hardware-efficient coherent digital receiver concept with feedforward carrier recovery for m-QAM constellations," *J. Lightwave Technol.*, vol. 27, no. 8, pp. 989–999, Apr 2009. [Online]. Available: http://jlt.osa.org/abstract.cfm?URI=jlt-27-8-989

[14] D. Perels, S. Haene, P. Luethi, A. Burg, N. Felber, W. Fichtner, and H. Bolcskei, "ASIC implementation of a MIMO-OFDM transceiver for 192 mbps WLANs," in *Proceedings of the 31st European Solid-State Circuits Conference, 2005. ESSCIRC 2005.*, Sept 2005, pp. 215–218.

[15] K. Zhong, X. Zhou, T. Gui, L. Tao, Y. Gao, W. Chen, J. Man, L. Zeng, A. P. T. Lau, and C. Lu, "Experimental study of PAM-4, CAP-16, and DMT for 100 gb/s short reach optical transmission systems," *Opt. Express*, vol. 23, no. 2, pp. 1176–1189, Jan 2015. [Online]. Available: http://www.opticsexpress.org/abstract.cfm?URI=oe-23-2-1176

[16] A. V. Oppenheim and R. W. Schafer, *Discrete-time signal processing*. Pearson Education, 2014.

[17] M. S. Faruk and K. Kikuchi, "Adaptive frequency-domain equalization in digital coherent optical receivers," *Opt. Express*, vol. 19, no. 13, pp. 12 789–12 798, Jun 2011. [Online]. Available: http://www.opticsexpress.org/abstract.cfm?URI=oe-19-13-12789

[18] J. L. Wei, Q. Cheng, R. V. Penty, I. H. White, and D. G. Cunningham, "Analysis of complexity and power consumption in DSP-based optical modulation formats," in *Advanced Photonics for Communications*. Optical Society of America, 2014, p. SM2D.5. [Online]. Available: http://www.osapublishing.org/abstract.cfm?URI=SPPCom-2014-SM2D.5

[19] J. Leibrich and W. Rosenkranz, "Frequency domain equalization with minimum complexity in coherent optical transmission systems," in *Optical Fiber Communication Conference*. Optical Society of America, 2010, p. OWV1. [Online]. Available: http://www.osapublishing.org/abstract.cfm?URI=OFC-2010-OWV1